



UNIVERSITY OF LEEDS

This is a repository copy of *Surface Functional Groups and Graphitization Degree of Soot in the Sooting History of Methane Premixed Flame*.

White Rose Research Online URL for this paper:

<https://eprints.whiterose.ac.uk/172717/>

Version: Accepted Version

Proceedings Paper:

Liu, Y orcid.org/0000-0002-9367-3532, Lv, G, Fan, C et al. (2 more authors) (2017) Surface Functional Groups and Graphitization Degree of Soot in the Sooting History of Methane Premixed Flame. In: SAE Technical Paper Series. WCX™ 17: SAE World Congress Experience, 04-06 Apr 2017, Detroit, USA. SAE International .

<https://doi.org/10.4271/2017-01-1003>

This is protected by copyright. All rights reserved. This is an author produced version of a conference paper published in SAE Technical Papers. Uploaded in accordance with the publisher's self-archiving policy.

Reuse

Items deposited in White Rose Research Online are protected by copyright, with all rights reserved unless indicated otherwise. They may be downloaded and/or printed for private study, or other acts as permitted by national copyright laws. The publisher or other rights holders may allow further reproduction and re-use of the full text version. This is indicated by the licence information on the White Rose Research Online record for the item.

Takedown

If you consider content in White Rose Research Online to be in breach of UK law, please notify us by emailing eprints@whiterose.ac.uk including the URL of the record and the reason for the withdrawal request.



eprints@whiterose.ac.uk
<https://eprints.whiterose.ac.uk/>

Surface Functional Groups and Graphitization Degree of Soot in the Sooting History of Methane Premixed Flame

Author, co-author (Do NOT enter this information. It will be pulled from participant tab in MyTechZone)

Affiliation (Do NOT enter this information. It will be pulled from participant tab in MyTechZone)

Abstract

The evolution of surface functional groups (SFGs) and the graphitization degree of soot generated in premixed methane flames are studied and the correlation between them is discussed. Test soot samples were obtained from an optimized thermophoretic sampling system and probe sampling system. The SFGs of soot were determined by Fourier transform infrared spectroscopy (FT-IR) and X-ray photoelectron spectroscopy (XPS) after removing the soluble impurities from the soot samples, while the graphitization degree of soot was characterized by Raman spectrum and electron energy loss spectroscopy (EELS). The results reveal that the number of aliphatic C–H groups and C=O groups shows an initial increase and then decrease in the sooting history. The large amount of aliphatic C–H groups and small amount of aromatic C–H groups in the early stage of the soot mass growth process indicate that aliphatic C–H groups make a major contribution to the early stage of soot mass growth. The higher graphitization degree of soot appears at low height above the burner when the graphite core is formed. The graphitization degree of soot rapidly decreases in the early mass growth stage then increases in the maturation process. The results from transmission electron microscopy (TEM), SFGs, and the graphitization degree verify the assumption that the nascent soot consists of a graphite-like core and an aliphatic shell. There is a strong correlation between SFGs and graphitization degree in the early stage of the soot mass growth process. During the soot maturation process, the correlation between SFGs and graphitization degree weakens. The SFGs may be related to the aggregate soot particle properties, such as fractal dimension.

Introduction

Soot is often an undesirable combustion product of hydrocarbon fuel combustion systems. We define soot as the solid core. The formation and evolution of soot consists of complex and concurrent physical and chemical processes. During the sooting history, the physical and chemical properties of soot show dramatic changes owing to their dependence on fuel and synthesis/combustion conditions [1–7]. The study of soot properties is thus important for both obtaining information on their origin and determining their fate when emitted from combustion systems. In previous studies, the surface functional groups (SFGs) at different soot history for premixed flames have been investigated using micro-Fourier transform infrared spectroscopy (μ -FT-IR) [8,9]. The results suggested that the soot formed in premixed flat flames can contain a substantial amount of aliphatic components, indicating the extremely important role of aliphatic C–H groups in the soot growth process. The presence of aliphatic components affects intrinsic particle properties, including mass density and reactive surface site density, and may influence

surface growth rates and coagulation behavior. However, the soot samples in these studies did not undergo pretreatments to remove the soluble impurities on the soot surface. These soluble impurities, such as polycyclic aromatic hydrocarbons (PAHs), include a large number of aromatic C–H groups [10]. This may affect the results when quantifying SFGs by FT-IR and further affect the accuracy when developing new reaction models to predict the soot size and chemical composition.

In addition to the soot physicochemical properties, the potential correlations between the physical and chemical property parameters have also received attention [11–16]. Alfè et al. [13] concluded that there is a structure–property relationship between the soot nanostructure and bulk properties, such as the amount of C–H groups. They found that the population of C–H groups decreases with increasing fringe length of soot during the soot maturation process. Cancado et al. found that the graphitization degree is proportional to the in-plane crystallite size [17,18]. Franklin et al. [19] discovered that the graphitization process is related to the presence of large quantities of hydrogen in the carbon material. Meanwhile, according to the studies of Dibbins and his colleagues [20,21], the carbonization process of liquid-like precursor particles is accompanied with the decrease in hydrogen mole fraction from 0.35 to 0.15. It seems that there is a correlation between graphitization degree of soot and SFGs. In this context, optimized thermophoretic sampling and probe sampling techniques were used to obtain soot samples, and the samples were then analyzed by high-resolution transmission electron microscopy (HRTEM), Raman spectroscopy, electron energy loss spectroscopy (EELS), FT-IR, and X-ray photoelectron spectroscopy (XPS). There are two main objectives in this study: (1) To obtain information about the SFGs and graphitization degree of soot in the sooting history of premixed methane flame, especially the evolution of SFGs of soot samples after removing soluble impurities. (2) To try to determine the relationship between graphitization degree of soot and SFGs.

Experimental

Burner

The rich premixed methane/oxygen flames were produced with a flat-flame burner (Holthuis & Associates, Sebastopol, USA). An external shroud of nitrogen with a flow rate of 30 L/min was supplied around the plug to shield the flame from perturbations by atmospheric air. Details of the McKenna burner have been described elsewhere [8,9]. In this study, two premixed methane/oxygen flames with different cold mixture velocities of 6 and 8 cm/s were chosen to compare and validate the experimental results. The flow rates of the gas components were accurately set by a digital mass flow controller with

accuracy of 0.35% F.S. (Sevenstar, CS200A). The burner was mounted on a motorized translation stage with an accuracy of 0.01 mm so that it could be moved vertically relative to the fixed sampling system, and a constant temperature cooling water tank was used to maintain the initial mixture gas temperature (300 K).

Sampling system

Soot sampling for transmission electron microscopy (TEM) analysis was performed by an improved thermophoretic sampling particle diagnostic (TSPD). An electric cylinder (Festo, DNCE-32-320-LAS) was used to ensure the exact exposure time. The electric cylinder was based on an innovative tubular linear motor and can offer full programmable, closed-loop position, and acceleration and speed control. Compared with traditional double-acting pneumatic cylinders [22,23], the electric cylinder can provide a more accurate position with a positioning repeatability of 0.02 mm. An exposure time of approximate 20 ms was used for a large number of tests, and a series of parameters for the electric cylinder were set to obtain the anticipated exposure time (e.g., an acceleration of 120 m s^{-2} and a velocity of 3 m s^{-1}). Considering the effects of the probe thickness and vibration on the disturbance of flames, self-locking tweezers with a tip diameter of 0.1 mm were used to replace the traditional two-layer holder. TEM grids were clamped by tweezers then inserted into the flame to obtain particle samplings at heights above the burner (HAB) of 2, 5, 10, 15 and 25 mm. A customized fast-response R-type thermocouple (Pt/Pt-13%Rh with the junction bead diameter of 150 μm) loaded on the DNCE-LAS electric cylinder was used to measure the flame temperature at different radial and axial directions using a fast-insertion procedure. After every insertion of the thermocouple, the soot rapidly aggregated on the surface of the junction bead, which resulted in an apparent decrease in temperature owing to radiation. Therefore, a cleaning procedure was performed after the insertion of the thermocouple by burning out the soot on the surface of the thermocouple in a flame with C/O = 0.2. Because of the clean surface of the thermocouple, radiation correction was not used in our experiments. The error of the thermocouple was $\pm 50 \text{ K}$ because of uncertainties in the thermocouple measurement and radiation correction, and the experimental uncertainty was determined from three repeated measurements of a temperature profile.

Additionally, soot samples for other analyses were obtained by an *in situ* sample probe. The major difference between our experiment and previous studies [8,9] is that a smaller probe with a diameter of 3.175 mm was used to minimize the effect of the probe on the flame temperature. The probe was positioned horizontally over the burner with the orifice on the central axis of the burner. At the same time, cold nitrogen flowed through the sample probe to dilute the particles that enter the probe through a 0.15-mm-diameter pinhole. The pressure gradient inside the tube was controlled and the pressure at the pinhole determines the sampling dilution ratio [24–26]. The particle samples were collected on Teflon-based filters (R2PL047, PALL, USA) for HAB = 5, 8, 10, 15, and 25 mm, from which the soot was separated by ultrasonic wave treatment in dichloromethane (DCM) solvent at room temperature. The sediment of the soot was obtained from the DCM suspension by centrifugal separation. After removal of the DCM supernatant, the ultrasonic wave treatment and centrifugal separation were repeated two more times in DCM to remove any remaining soluble impurities from the soot. The resulting soot samples were dried under nitrogen and then sealed in a glass bottle prior to analysis. In this study, we define soot as the dry soot without any soluble impurities.

Fourier transform infrared spectroscopy (FT-IR)

Page 2 of 9

FT-IR spectroscopy was employed to identify the functional groups and to quantify the relative amounts of functional groups on the soot surface. A Nicolet Nexus 470 FT-IR spectrometer with a resolution of 1 cm^{-1} was used with the KBr tablets. The KBr tablets were prepared by mixing and grinding the soot in KBr pellets (0.5 wt%) and the mixed-dispersions were compressed at 10 Ton for 5 min into a thin disk. Spectra were baseline-corrected and smoothed prior to analysis. A continuous background was subtracted from the sample spectra in the baseline correction procedure. The absorbance spectra were generated using the OMNIC software package (Thermo Nicolet). Three spectra were acquired for each sample to ensure reproducibility, and the variations in the FT-IR measurements were found to be less than 5%.

Transmission electron microscopy (TEM)

TEM images were obtained using an HRTEM (Philips Tecnai F20) with a point resolution of 0.248 nm operating at 200 kV. The magnifications were used in the TEM inspections: 20,000 \times to image the soot morphology. EELS were recorded with a Gatan Image Filter (GIF Tridiem; Gatan, USA) attached to the Philips Tecnai F20. For each sample, the EELS spectra were obtained for 10 randomly selected primary particles using the area scanning method. The integrated intensity ratio of the π^* peak and the δ^* peak (I_{π^*}/I_{δ^*}) was determined by the average value of obtained spectrum.

X-ray photoelectron spectroscopy (XPS)

The concentrations of oxygenated SFGs were determined by X-ray photoelectron spectroscopy (XPS) (Perkin-Elmer PHI-1600 ESCA) using a MgK α X-ray source. The binding energies were calibrated using C1s peak of contaminant carbon (BE = 284.6 eV) as an internal standard. The XPS results from three different sections of the soot sample were averaged and an uncertainty of less than 7% was obtained.

Raman spectroscopy

Raman spectrometer (Renishaw RM1000) was used to conduct complementary characterization of the soot nanostructure. The Raman spectra were recorded over a wavelength number range of 900–2000 cm^{-1} . The excitation laser was an Ar ion laser with a wavelength of 514.5 nm and source power of 20 mW. For each sample, the magnitude of scanning area was 2 μm in diameter. Raman spectra were recorded at approximately 10 positions with an acquisition time of 60 s and a hardware accumulation of 3 times to reduce noise in the spectra.

Results and discussion

Surface functional groups of soot

FT-IR spectroscopy was used to probe the nature and content of C–H and C=O groups on the soot surface. A typical baseline-corrected, smoothed FT-IR spectrum of sampling soot at HAB = 5 mm is shown in Fig. 1. The peaks and their assignments are given in Table 1. The absorbance band at 1720 cm^{-1} corresponds to the carbonyl group (C=O), while the C–H stretching features at 2960, 2920 and 2860 cm^{-1} are assigned to aliphatic groups [27,28]. According to the studies of Ivleva and his colleagues [29], the functional groups are most likely to be bound on the soot surface, and this theory is also supported by Cain et al. [8,9]. Therefore, we assume that the SFGs

detected by FT-IR measurements are mostly located on the soot surface, especially for the sampling soot after soluble impurities are removed. Given that several factors, such as the thickness and concentration of the KBr pellet, and the quality of sampling soot, can affect absolute peak height comparison between different spectra, quantitative analysis of the relative functional group abundances was performed using a set of standards suggested by Cain et al. [8]. The molar concentrations of groups relative to the aromatic C–H (3050 cm^{-1}) group were determined.

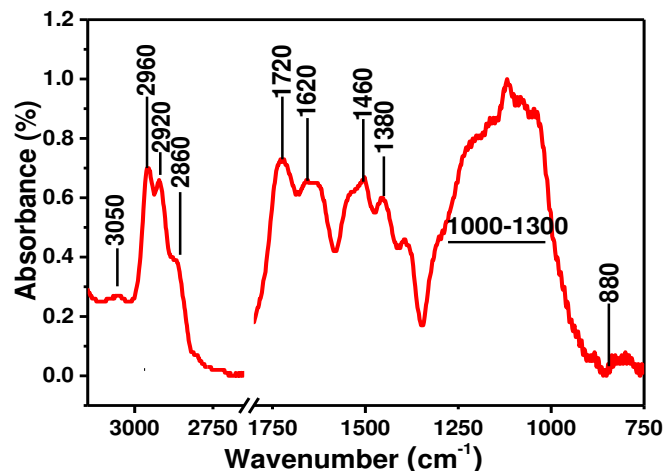


Figure 1. Typical baseline corrected, smoothed infrared spectrum (mixture gas velocity = 6 cm/s and height above the burner = 5 mm).

Table 1. FT-IR peaks observed for soot collected along with assignments

Peak/ cm^{-1}	Assignments
3050	Aromatic C–H stretch
2960	Alkane CH_3 asymmetric stretch
2920	Alkane CH_2 asymmetric stretch
2860	Alkane CH_3 symmetric stretch
1720	Carbonyl C=O
1620	Aromatic C=C
1460	Unsaturated C–H stretch
880	Substituted aromatic C–H

Figure 2 shows the relationship between the concentration ratios of [aliphatic C–H]/[aromatic C–H] and [C=O]/[aromatic C–H] with the increase of HAB for two different flames. Several important observations can be made from this plot. First, the concentration ratios of [aliphatic C–H]/[aromatic C–H] in our experiments are much larger than the results of Cain et al. [8], which is due to the removal of the soluble impurities from the soot particles. The soluble organic material on soot particles primarily composes of aliphatic hydrocarbon, polycyclic aromatic hydrocarbons (PAHs), nitric- and oxi-PAHs, including a large amount of aromatic and aliphatic C–H groups, but the concentration of aromatic C–H groups is larger than that of aliphatic C–H groups [30,31]. Therefore, removing the soluble organic material results in the increase in the concentration ratio of [aliphatic C–H]/[aromatic C–H]. Second, the concentration ratios of [aliphatic C–H]/[aromatic C–H] and [C=O]/[aromatic C–H] initially increase and then decrease with increasing flame height. Soot is highly oxidized at a flame height of 5 mm due to higher temperature, indicating that aliphatic C–H groups and C=O groups on the soot surface are oxidized rather than the aromatic C–H group. Nuclear soot formed at this height (see Fig. 3) and the surface of nuclear soot may be aromatic rather than aliphatic. Thus, the concentration ratios of [aliphatic C–H]/[aromatic C–H] and [C=O]/[aromatic C–H] at this

Page 3 of 9

height are less than the other heights. The concentration ratios then rapidly increase with increasing HAB from 5 to 10 mm. The nuclear soot rapidly grows by subsequent reactions of growth species on the soot surface during this stage. There is a considerable amount of experimental work published on the growth species on the soot surface. For example, Dobbins and his colleagues [20,32] explored the relationship between soot growth and the stabilomer PAHs by means of the laser microprobe mass spectrometry. They found that the PAH content is similarly measured in subsequent aerosol mass spectrometry of flame generated soot. Maricq et al. [33] discovered that the chemical fingerprint and its relative variance to flame conditions appears consistent with the accepted hydrogen-abstraction-carbon-addition (HACA) mechanism for soot growth via acetylene addition and PAH condensation. However, Wang et al. [5,8] pointed out that the aliphatic C–H groups play an important role in the soot early mass growth process. Our observation is similar to the conclusions of Wang et al. The observation in this study may indicate that the HACA mechanism is not major pathways for soot mass growth process. The concentration ratios of [aliphatic C–H]/[aromatic C–H] and [C=O]/[aromatic C–H] decrease with increase of HAB from 10 to 25 mm, where the coagulation and agglomeration processes are the main factors that affect soot mass growth. According to the assumption that mature soot particles include an aliphatic shell, coagulation and agglomeration of soot particles block a large number of active sites that can adsorb aliphatic C–H SFGs, resulting in the decrease in the concentration ratios. Third, the concentration ratio of [aliphatic C–H]/[aromatic C–H] is much larger than that of [C=O]/[aromatic C–H], which also indicates the extremely important functions of aliphatic C–H groups in the soot growth process. Finally, an obvious difference is observed compared

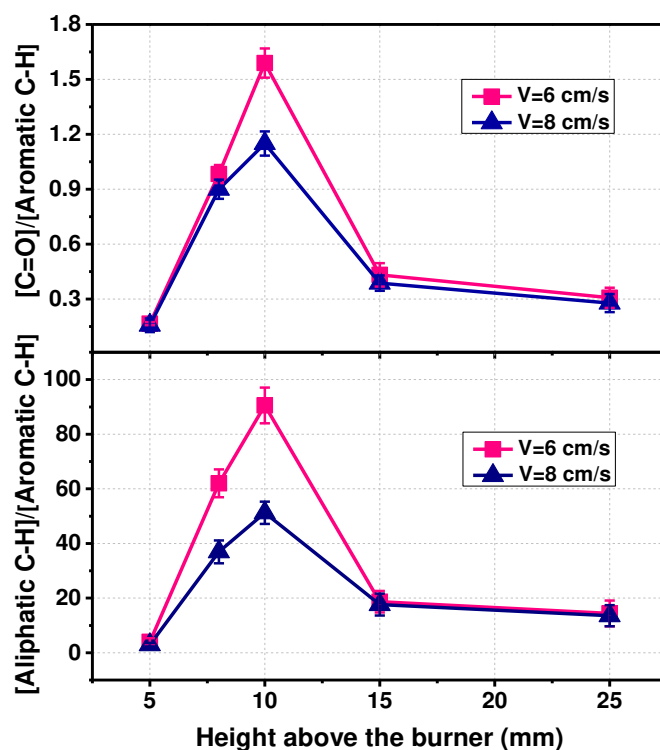


Figure 2. Relative concentrations of C=O and aliphatic C–H groups obtained from FT-IR spectra as a function of height above the burner (HAB). The error bars represent the standard error. V is the mixture gas velocity.

with other studies: both the concentration ratios of [aliphatic C–H]/[aromatic C–H] and [C=O]/[aromatic C–H] with the mixture gas velocity equal to 6 cm/s are larger than those with the mixture gas

velocity equal to 8 cm/s. However, the results are reasonable because soot becomes more carbonized and more functional groups are oxidized as the flame temperature increases. Moreover, the discrepancy among experiment results may result from the pretreatment process, which removes the soluble impurities from soot particles.

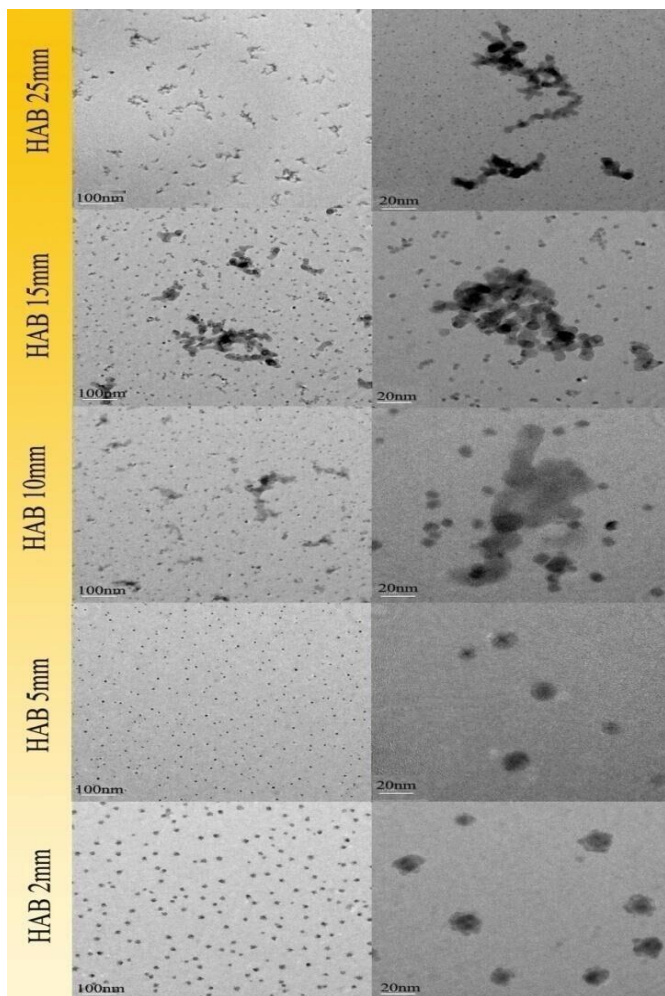


Figure 3. TEM images of soot particles at different heights above the burner.

As well as FT-IR spectroscopy, we also used X-ray photoelectron spectroscopy (XPS) to determine the concentrations of oxygenated SFGs to verify the results from FT-IR spectroscopy. A typical narrow scan of C 1s peak is shown in Fig. 4. Peak deconvolution and fitting to experimental data [34–36] indicate that the C 1s peak can be well fitted by three peaks: the C–OH groups at 286.3 eV, the C=O groups at 288.5 eV, and the C–C sp² bond at 284.5 eV. The concentrations of C–OH and C=O SFGs obtained from XPS spectra at different heights are shown in Fig. 5. The figures of the oxygenated SFGs with the change of flame height are similar to the results from FT-IR spectroscopy, which show an initial increase and then a decrease with increasing HAB. Oxygenated SFGs such as C=O and C–OH groups are inherently generated as intermediates upon partial oxidation of soot [35]. Soot can be partially oxidized by species such as OH and O, producing oxygenated functional groups as intermediates. Because the highest flame temperature with a mixture gas velocity equal to 8 cm/s is larger than that with a mixture gas velocity equal to 6 cm/s, the concentrations of oxygenated functional groups decrease faster with higher flame temperature. This is a competitive result between complete oxidation and partial oxidation. A higher flame temperature

gives a more intense oxidation reaction, resulting in a small drop in the concentrations of oxygenated functional groups.

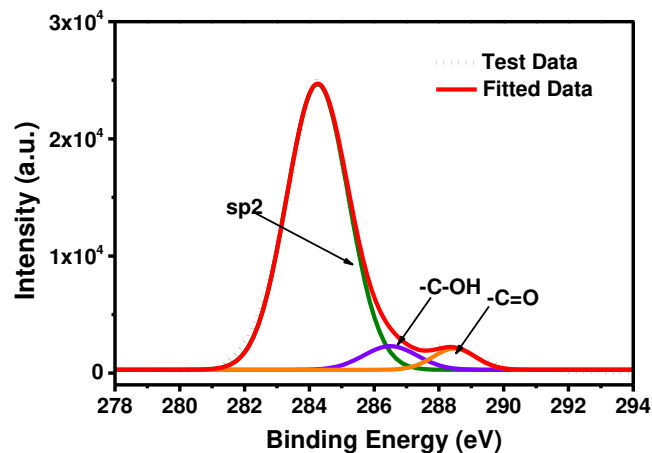


Figure 4. Typical XPS C 1s narrow spectrum of soot (mixture gas velocity = 8 cm/s and height above the burner = 25 mm)

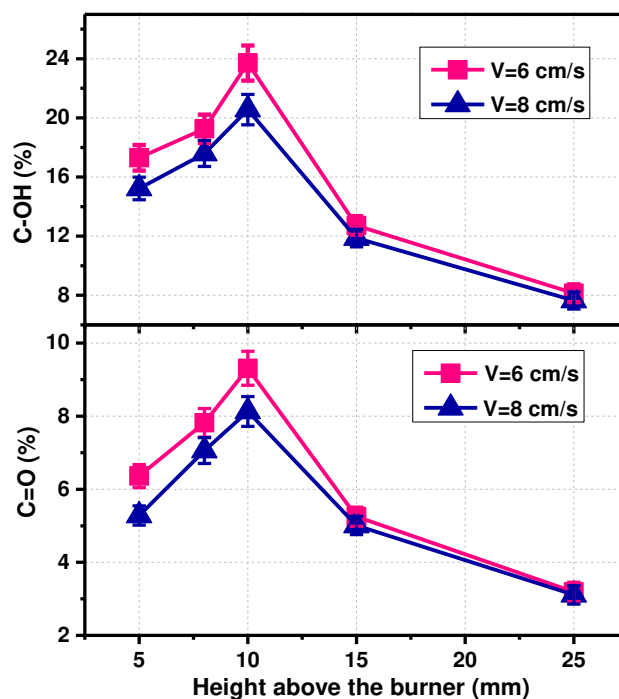


Figure 5. Concentrations of C–OH and C=O SFGs determined by XPS spectra as a function of height above the burner. V is the mixture gas velocity.

Graphitization degree of soot

The graphitization degree is an important parameter of soot particles that indicates the disordered graphitic content, and is also strongly correlated with the in-plane crystallite size [37,38]. Typical methods to measure the graphitization degree of soot include Raman spectroscopy and EELS. The Raman signals of graphite crystals result from lattice vibrations and are very sensitive to the degree of structural disorder, while EELS gives very high spatial resolution and almost single atom compositional sensitivity. In our study, both methods were used for verification and EELS was used to obtain information to determine the graphitization degree of soot at low flame heights (HAB < 5 mm). The Raman spectrum at different

flame heights can be seen in Fig. 6. As noted, all Raman spectra exhibit two characteristic peaks: D (defect) peaks at 1350 cm^{-1} and G (graphite) peaks at 1580 cm^{-1} . The D peak originates from the breakdown of the selection rules for graphene atoms in the breathing vibrational mode, with an intensity that depends on the disorder level of the graphitic structure, and the G peak is related to a C-C stretching motion along the longitudinal axis of the graphitic plane [39,40]. As recommended by Li et al. [41] and Song et al. [39], the integrated intensity ratio of D peak and G peak (I_D/I_G) is used to characterize the graphitization degree of soot. A larger ratio means a lower graphitization degree. Interestingly, the peak at 1350 cm^{-1} has a shoulder peak at 1200 cm^{-1} only at HAB = 5 mm. Dippel et al. [42] observed this band at 1190 cm^{-1} in the Raman spectrum of flame soot and tentatively attributed it to sp^2 - sp^3 bonds or C-C and C=C stretching vibrations of polyene-like structures. The integrated intensity ratio of the π^* peak and the δ^* peak (I_{π^*}/I_{δ^*}) determined by the EELS spectrum is used to characterize the sp^2 hybridization content of the soot particle. A larger ratio means higher sp^2 hybridization, which also indicates a higher graphitization degree of soot. I_{π^*}/I_{δ^*} was obtained by calculating the average value measured from 10 randomly selected primary soot particles in the TEM images. I_D/I_G and I_{π^*}/I_{δ^*} determined by EELS spectra as a function of height for both flames are shown in Figs. 7a and 7b, respectively. From HAB = 2 to 5 mm, only single soot particles are formed (as shown in Fig. 3). Condensed-phase soot particles of loose structure and relatively large diameter are initially formed at a very low height (HAB = 2 mm). These particles are surrounded by a halo or some translucent species and have a liquid-like nature and nebulous boundaries, corresponding to the lowest graphitization degree. The soot particle with higher graphitization degree appears at HAB = 5 mm, where the stabilized nuclear soot is formed but the oxidation reaction is also strong owing to higher flame temperature. Obviously, a proportional relationship between the graphitization degree and the in-plane crystallite size is inappropriate for nuclear soot because nuclear soot with the higher graphitization degree does not represent a larger in-plane crystallite size. However, this conclusion is very similar to the assumption by Cain et al [8], who proposed that nascent soot consists of a graphitic-like core and an aliphatic shell. The graphitization degree of soot then decreases significantly from HAB = 5 to 10 mm owing to the large amount of newly formed soot particles as well as the rapid growth of the generated soot particles. After the appearance of cluster-phase particles or chain-like particles (HAB = 10 to 25 mm), the graphitization degree of soot increases in the soot maturation process corresponding to the larger in-plane crystallite size of the primary particle.

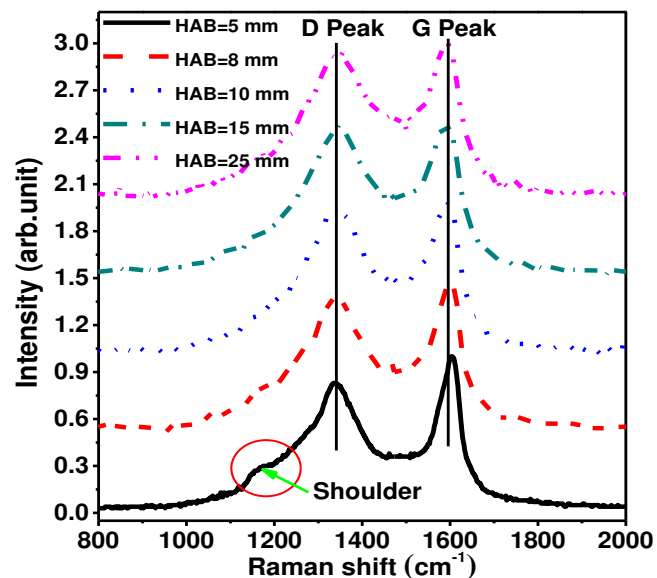


Figure 6. Raman spectrum at different heights above the burner (HAB).

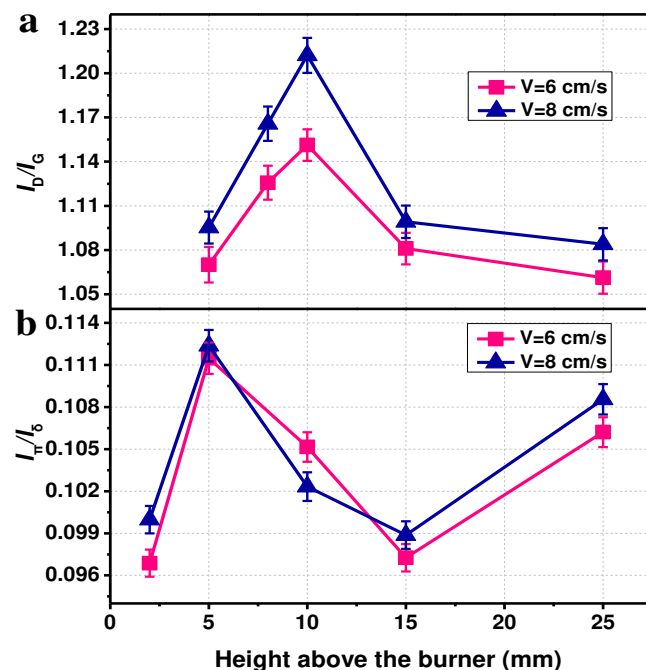


Figure 7. I_D/I_G determined by Raman spectra and I_{π^*}/I_{δ^*} determined by EELS spectra as a function of height above the burner.

Relationship between soot graphitization and SFGs

The normalized concentration of C-OH, aliphatic C-H, and C=O SFGs as a function of I_D/I_G is shown in Fig. 8. The history of soot generated in the premixed flame can be described in three stages. The first stage is the initial soot nucleation, corresponding to the region HAB < 5 mm. The results from EELS and TEM show the formation of the graphite core. A laser-induced fluorescence and photo ionization aerosol mass spectrometry (PIAMS) analysis indicates that there is a large amount of PAHs and other intermediates in this region [43]. We also observed the existence of unsaturated C-H bonds (the shoulder peak at 1200 cm^{-1}). Both PAHs and unsaturated C-H groups play important roles in the formation process of graphite core. The second stage from $5\text{ mm} < \text{HAB} < 10\text{ mm}$ is soot growth, which

mostly occurs by the addition of growth species, especially aliphatic C–H groups. A close correlation was found between the graphitization degree and the SFGs. Soot with a high graphitization degree has a low concentration of SFGs. On the one hand, the large number of intermediates provides enough growth species that react with SFGs to significantly change the soot morphology and graphitization degree. On the other hand, the decreasing graphitization degree also provides a large number of active sites accelerating soot growth. The third stage is soot growth by coalescence and agglomeration. The large loss of active sites by coalescence and agglomeration causes the significant decrease of SFGs. The disordered structure gradually disappears in the maturation processes, changing to an ordered shell–core structure and corresponding to the increase in graphitization degree. The correlation between SFGs and graphitization degree in the third stage is not as close as that in the second stage, although soot with a high graphitization degree also has a low concentration of SFGs. In this stage, it seems that the morphology of the soot aggregates, such as the fractal dimension, may play an important role in determining the SFGs.

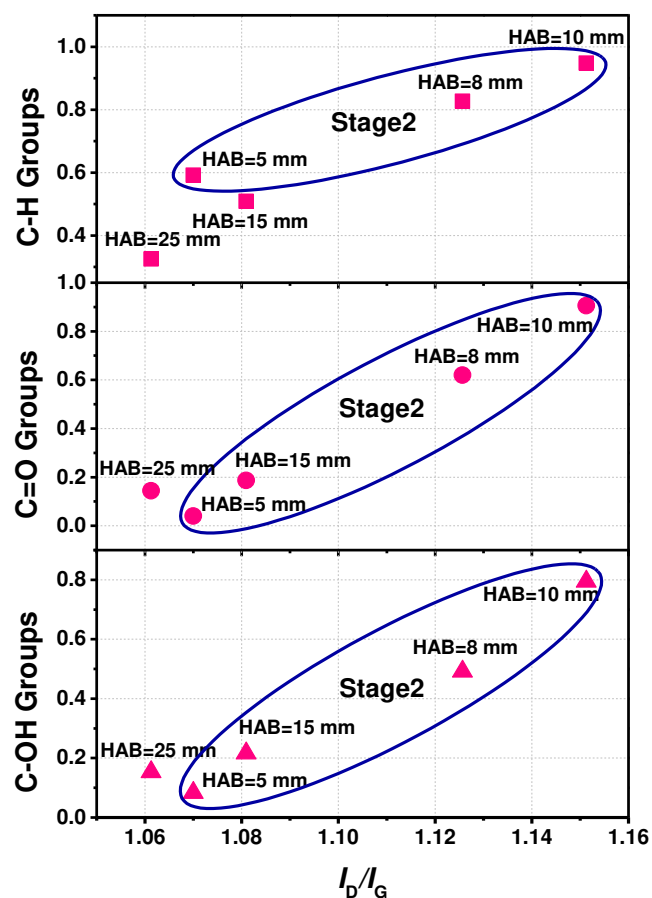


Figure 8. Normalized concentration of SFGs as a function of ratio I_D/I_G at different heights above the burner (HAB). Mixture gas velocity (V) = 6 cm/s

Conclusions

The soot generated in premixed methane flames was sampled using an optimized thermophoretic sampling system and a probe sampling system. The evolution of SFGs and graphitization degree of the soot were studied by FT-IR, XPS, Raman spectroscopy, and EELS. The concentration ratios of [aliphatic C–H]/[aromatic C–H] and

[C=O]/[aromatic C–H] initially increase and then decrease with increasing HAB. The lower concentration ratio of [aliphatic C–H]/[aromatic C–H] after soot nucleation indicates that the aromatic C–H groups make a major contribution to the soot nucleation process, and the rapid increase of the aliphatic C–H groups in the early stage of the soot mass growth process indicates the extremely important role of aliphatic C–H groups in this stage. In general, most models assume that nascent, growing soot particles are aromatic in nature and soot mass growth follows the hydrogen-abstraction-carbon-addition (HACA) mechanism with rate constants analogous to gas-phase reactions of small aromatics [34]. The observation in this study may indicate that the HACA mechanism is not major pathways for soot mass growth process. However, this observation supports the conclusion obtained from the FT-IR study of soot generated in a similar flame [44].

The results from Raman spectroscopy and EELS show that the higher graphitization degree appears at the lower HAB, indicating the soot core is more graphite-like. The graphitization degree of soot decreases in the early stage of the soot mass growth stage and then slightly increases in the soot maturation stage of aliphatic C–H groups in this stage.

There is a strong correlation between SFGs and graphitization degree in the early soot mass growth stage. A lower graphitization degree of soot represents more reactive sites, which causes the increase in SFGs by the adsorption of growth species to the soot surface.

References

1. Vander Wal, R. L., Yezerets, A., Currier, N. W., Kim, D. H. et al., "HRTEM Study of diesel soot collected from diesel particulate filters," *Carbon* 45(1):70–77, 2007.
2. Vander Wal, R. L. and Tomasek, A. J., "Soot oxidation: dependence upon initial nanostructure," *Combustion and Flame* 134(1):1–9, 2003.
3. Li, Z., Song, C., Song, J., Lv, G., Dong, S. et al., "Evolution of the nanostructure, fractal dimension and size of in-cylinder soot during diesel combustion process," *Combustion and Flame* 158(8):1624–1630, 2011.
4. Mungekar, H. P. and Atreya, A., "Effect of partial premixing on the sooting structure of methane flames," *Combustion and Flame* 144(1):336–348, 2006.
5. Wang, H., "Formation of nascent soot and other condensed-phase materials in flames," *Proceedings of the Combustion Institute* 33(1):41–67, 2011.
6. Feng, X., Huo, M., Lee, C. F. and Liu, H., "The Effects of EGR and Injection Timing on the Engine Combustion and Emission Performances Fueled by Butanol-Diesel Blends," *SAE International Journal of Engines* 2011-01-2473, 2012, doi:10.4271/2011-01-2473.
7. O'Connor, J. and Musculus, M., "Post injections for soot reduction in diesel engines: A review of current understanding," *SAE International Journal of Engines* 2013-01-0917, 2013, doi:10.4271/2013-01-0917.
8. Cain, J. P., Gassman, P. L., Wang H. and Alexander, L., "Micro-FTIR study of soot chemical composition-evidence of aliphatic hydrocarbons on nascent soot surfaces," *Physical Chemistry Chemical Physics* 12(20):5206–5218, 2010.
9. Cain, J. P., Camacho, J., Phares, D. J., Wang, H. et al., "Evidence of aliphatics in nascent soot particles in premixed ethylene flames," *Proceedings of the Combustion Institute* 33(1):533–540, 2011.

10. Mckinnon, J. T., Meyer, E. and Howard, J. B., "Infrared analysis of flame-generated PAH samples," *Combustion and Flame* 105(1):161–166, 1996.
11. Esangbedo, C., Boehman, A. L. and Perez, J. M., "Characteristics of diesel engine soot that lead to excessive oil thickening," *Tribology International* 47:194–203, 2012.
12. La Rocca, A., Di Liberto, G., Shayler, P. J. and Fay, M. W., "The nanostructure of soot-in-oil particles and agglomerates from an automotive diesel engine," *Tribology International* 61:80–87, 2013.
15. Döpelheuer, A., "Quantities characteristics and reduction potentials of aircraft engine emissions," SAE Technical Paper 2001-01-3008, 2001, doi:[10.4271/2001-01-3008](https://doi.org/10.4271/2001-01-3008).
16. Vander Wal, R. L., "Soot nanostructure: Definition, quantification and implications," SAE Technical Paper 2005-01-0964, 2005, doi:[10.4271/2005-01-0964](https://doi.org/10.4271/2005-01-0964).
17. Cancado, L. G., Takai, K., Enoki, T., Endo, M. et al., "Measuring the degree of stacking order in graphite by Raman spectroscopy," *Carbon* 46(2):272–275, 2008.
18. Cancado, L. G., Takai, K., Enoki, T. and Endo, M., "General equation for the determination of the crystallite size l_a , of nanographite by raman spectroscopy," *Applied Physics Letters* 88(16):163106–163106–3, 2006.
19. Franklin, R. E., "Crystallite growth in graphitizing and non-graphitizing carbons," *Physical and Engineering Sciences* 1097(209):196–218, 1951.
20. Dobbins, R. A., Fletcher, R. A., and Chang, H. C., "The evolution of soot precursor particles in a diffusion flame," *Combustion and flame* 115(3):285–298, 1998.
21. Dobbins, R. A., Govatzidakis, G. J., Lu, W., Schwartzman, A. F. et al., "Carbonization rate of soot precursor particles," *Combustion science and technology* 121(1):103–121, 1996.
22. Lee, J., Altman, I. and Choi, M., "Design of thermophoretic probe for precise particle sampling," *Journal of Aerosol Science* 39(5):418–431, 2008.
23. Dobbins, R. A. and Megaridis, C. M., "Morphology of flame-generated soot as determined by thermophoretic sampling," *Langmuir* 3(2):254–259, 1987.
24. Zhao, B., Yang, Z., Li, Z., Johnston, M. V. et al., "Particle size distribution function of incipient soot in laminar premixed ethylene flames: effect of flame temperature," *Proceedings of the Combustion Institute* 30(1):1441–1448, 2005.
25. Zhao, B., Yang, Z., Johnston, M. V., Wang, H. et al., "Measurement and numerical simulation of soot particle size distribution functions in a laminar premixed ethylene-oxygen-argon flame," *Combustion and Flame* 133(1):173–188, 2003.
26. Abid, A. D., Heinz, N., Tolmachoff, E. D., Phares, D. J. et al., "On evolution of particle size distribution functions of incipient soot in premixed ethylene–oxygen–argon flames," *Combustion and Flame* 154(4):775–788, 2008.
27. Mondragón, F., Molina, A. and Marsh, N. D. "Ft-ir and 1h nmr characterization of the products of an ethylene inverse diffusion flame," *Combustion and Flame* 146(1–2):52–62, 2006.
28. Santamaria, A., Yang, N., Eddings, E. and Mondragon, F., "Chemical and morphological characterization of soot and soot precursors generated in an inverse diffusion flame with aromatic and aliphatic fuels," *Combustion and Flame* 157(1):33–42, 2010.
29. Ivleva, N. P., Messerer, A., Yang, X., Niessner, R. et al., "Raman microspectroscopic analysis of changes in the chemical structure and reactivity of soot in a diesel exhaust aftertreatment model system," *Environmental Science and Technology* 41(10):3702–3707, 2007.
13. Alfè, M., Apicella, B., Barbella, R., Rouzaud, J. N. et al., "Structure–property relationship in nanostructures of young and mature soot in premixed flames," *Proceedings of the Combustion Institute* 32(1):697–704, 2009.
30. Collura, S., Chaoui, N., Azambre, B., Fingueneisel, G. et al., "Influence of the soluble organic fraction on the thermal behaviour, texture and surface chemistry of diesel exhaust soot," *Carbon* 43(3):605–613, 2005.
14. Bhardwaj, O. P., Lüers, B., Holderbaum, B., Koerfer, T. et al., "Utilization of HVO fuel properties in a high efficiency combustion system: Part 2: Relationship of soot characteristics with its oxidation behavior in DPF," *SAE International Journal of Fuels and Lubricants* 2014-01-2846, 2014, doi:[10.4271/2014-01-2846](https://doi.org/10.4271/2014-01-2846).
31. Chong, H. S., Aggarwal, S. K., Lee, K. O., Yang, S. Y. et al., "Experimental investigation on the oxidation characteristics of diesel particulates relevant to DPF regeneration," *Combustion Science and Technology* 185(1):95–121, 2013.
32. Dobbins, R. A., Fletcher, R. A., and Lu, W., "Laser microprobe analysis of soot precursor particles and carbonaceous soot," *Combustion and Flame* 100(1):301–309, 1995.
33. Maricq, M. M., "An examination of soot composition in premixed hydrocarbon flames via laser ablation particle mass spectrometry," *Journal of Aerosol Science* 40(10):844–857, 2009.
34. Frenklach, M. and Wang, H., "Detailed modeling of soot particle nucleation and growth." *Symposium (International) on Combustion* 23(1):1559–1566, 1991.
35. Vander Wal, R. L., Bryg, V. M. and Hays, M. D., "Fingerprinting soot (towards source identification): Physical structure and chemical composition," *Journal of Aerosol Science* 41(1):108–117, 2010.
36. Boehm, H. P., "Surface oxides on carbon and their analysis: a critical assessment," *Carbon* 40(2):145–149, 2002.
37. Vander Wal, R. L., Bryg, V. M. and Hays, M. D., "XPS analysis of combustion aerosols for chemical composition, surface chemistry, and carbon chemical state," *Analytical Chemistry* 83(6):1924–1930, 2011.
38. Sadezky, A., Muckenhuber, H., Grothe, H., Niessner, R. et al., "Raman microspectroscopy of soot and related carbonaceous materials: spectral analysis and structural information," *Carbon* 43(8):1731–1742, 2005.
39. Song, J., Alam, M., Boehman, A. L., and Kim, U., "Examination of the oxidation behavior of biodiesel soot," *Combustion and flame* 146(4):589–604, 2006.
40. Maricq, M. M., "Chemical characterization of particulate emissions from diesel engines: A review," *Journal of Aerosol Science* 38(11):1079–1118, 2007.
41. Li, Z., Song, C., Song, J., Lv, G. et al., "Evolution of the nanostructure, fractal dimension and size of in-cylinder soot during diesel combustion process," *Combustion and Flame* 158(8):1624–1630, 2011.
42. Dippel, B., Jander, H. and Heintzenberg, J., "NIR FT Raman spectroscopic study of flame soot," *Physical Chemistry Chemical Physics* 1(20):4707–4712, 1999.
43. Furuhashi, T., Kobayashi, Y., Hayashida, K. and Arai, M., "Behavior of PAHs and PM in a diffusion flame of paraffin fuels," *Fuel* 91(1):16–25, 2012.
44. Russo, C., Tregrossi, A., and Ciajolo, A., "Dehydrogenation and growth of soot in premixed flames," *Proceedings of the Combustion Institute* 35(2):1803–1809, 2015.

Contact Information

Ye Liu
State Key Laboratory of Engines
Tianjin University
Tianjin, China
Weijin Road 92, Nankai Distinct
yeliu@tju.edu.cn

Tianjin University
Tianjin, China
Weijin Road 92, Nankai Distinct
Tel: +86-22-27406840-8021
lvg@tju.edu.cn

Gang Lv
State Key Laboratory of Engines

Acknowledgments

This study was supported by the National Natural Science Foundation of China (No. 51476115) and the National Key Basic Research and Development Program (No. 2013CB228502), and the Tianjin Research Program of application Foundation and Advanced Technology (13JCZDJC35800).

Definitions/Abbreviations

SFGs	Surface functional groups
FT-IR	Fourier transform infrared spectroscopy
XPS	X-ray photoelectron spectroscopy
TEM	Transmission electron microscopy
HRTEM	High-resolution transmission electron microscopy
EELS	Electron energy loss spectroscopy
HAB	Height above the burner
TSPD	Thermophoretic sampling particle diagnostic
DCM	Dichloromethane
PIAMS	Photo ionization aerosol mass spectrometry

